Parity-Time Symmetric Nonlocal Metasurfaces: All-Angle Negative Refraction and Volumetric Imaging

Francesco Monticone,[1] Constantinos A. Valagiannopoulos,[2] and Andrea Alù[1,3,*]

[1]*Department of Electrical and Computer Engineering, The University of Texas at Austin, Austin, Texas 78712, USA*

[2]*Department of Physics, School of Science and Technology, Nazarbayev University, KZ-010000 Astana, Kazakhstan*

[3]*Center for Nanophotonics, FOM Institute for Atomic and Molecular Physics, Science Park 104, 1098 XG Amsterdam, The Netherlands*

(Received 23 October 2015; revised manuscript received 16 August 2016; published 25 October 2016)

Lens design for focusing and imaging has been optimized through centuries of developments; however, conventional lenses, even in their most ideal realizations, still suffer from fundamental limitations, such as limits in resolution and the presence of optical aberrations, which are inherent to the laws of refraction. In addition, volume-to-volume imaging of three-dimensional regions of space is not possible with systems based on conventional refractive optics, which are inherently limited to plane-to-plane imaging. Although some of these limitations have been at least theoretically relaxed with the advent of metamaterials, several challenges still stand in the way of ideal imaging of three-dimensional regions of space. Here, we show that the concept of parity-time symmetry, combined with tailored nonlocal responses, enables overcoming some of these challenges, and we propose the design of a loss-immune, linear, transversely invariant, planarized metamaterial lens, with reduced aberrations and the potential to realize volume-to-volume imaging.

DOI: 10.1103/PhysRevX.6.041018 Subject Areas: Metamaterials, Optics

I. INTRODUCTION

Imaging indicates the ability of accurately reproducing an ensemble of point sources from an "object space" into a different "image space." Although such regions of space are three dimensional (3D), conventional imaging systems cannot reproduce full 3D images without distortion; instead, the imaging process is usually performed on pairs of two-dimensional (2D) transverse planes. For example, when we look around us, our eyes create 2D images on the retina, while the crystalline lens is adjusted to focus objects on planes at different distances. It is well known that optical imaging systems generally suffer from different kinds of monochromatic aberrations (spherical, comatic, astigmatic, etc.), which practically prevent the realization of an ideal image, even for a single object plane [1]. Therefore, it is relevant to ask whether ideal, aberration-free 2D or 3D optical imaging is at all theoretically possible, consistent with the laws of reflection and refraction (throughout this paper, ideal imaging is intended in the sense of geometrical optics, i.e., still limited by diffraction). Interestingly, it was demonstrated by Maxwell [2] (and later generalized) that no optical system with a given focal length can realize aberration-free imaging of two, or more, distinct transverse planes, no matter how complicated the lens (or combination of lenses) is (see, e.g., Refs. [1,3] and references therein). Instead, an ideal optical system that performs aberration-free imaging of a 3D region of space is necessarily afocal. In such a device, known as an "absolute optical instrument," the optical length of any curve in the object space is preserved in the image space [1], hence performing ideal volume-to-volume imaging. For over a century, it was thought that the only real example of a *planar* absolute optical instrument was a plane mirror [1,4,5], which is, however, of limited interest since the image points are virtual [Fig. 1(a)]; i.e., they cannot be directly projected onto a screen without using an additional lens that would introduce aberrations.

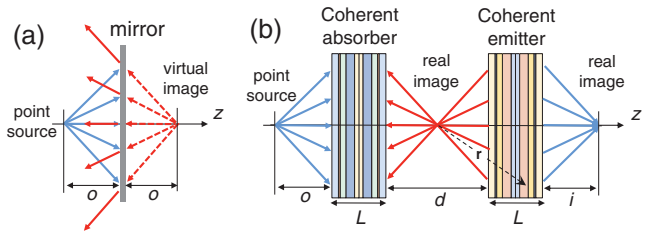

FIG. 1. Comparison of aberration-free imaging, under point-source illumination, by (a) a plane mirror and (b) the proposed nonlocal PT-symmetric lens, composed of an omnidirectional CPA paired with its time-reversed counterpart. In both cases, blue and red arrows denote waves propagating forward and backward, respectively, with respect to the positive z axis. Dashed arrows in (a) indicate rays originating from the virtual image.

*alu@mail.utexas.edu

Interestingly, with the advent of metamaterials, it has been shown that a planar slab having a negative index of refraction can realize, at least in principle, a transversely invariant, aberration-free, "perfect" lens [7,8]. Such a double-negative (DNG) slab indeed acts as a planar absolute optical instrument, but—different from a mirror—it produces *real* images of the 3D object space. In addition, different from any other lens previously devised, a DNG lens is able to overcome Abbe's diffraction limit of conventional optical imaging systems, hence opening the possibility of realizing images with ideally unlimited transverse resolution [8]. Although this fact has generated much interest in the scientific community, it was soon realized that such extreme imaging properties inevitably come at the expense of significantly increased sensitivity to losses, granularity, and other nonidealities, which are unavoidable in any practical implementation [9,10]. Besides, as confirmed by different numerical and experimental observations [10,11], the amplification of the evanescent spectrum, while supporting subdiffractive transverse resolution, inevitably determines strong resonant fields at the exit interface of the DNG lens, which makes it difficult to distinguish the images of different point sources along the longitudinal direction. In other words, in an ideal DNG lens, the improvement in *transverse* resolution comes at the cost of reduced *longitudinal* resolution. All these issues have so far hindered the applicability of DNG lenses in practical scenarios, and several alternative solutions have been investigated to realize negatively refracting lenses without negative-index materials, based, for example, on phase conjugation in parametrically modulated or nonlinear surfaces [12,13], or higher-order diffraction in photonic crystal slabs [14,15]. While these solutions offer some advantages compared to DNG lenses, they are affected by other limitations that may fundamentally hamper their performance: Phase conjugating lenses suffer from efficiency issues, as well as strong sensitivity to losses and other nonidealities, whereas photonic-crystal designs, not being transversely homogeneous, are limited in the transverse resolution that they can achieve. In addition, metamaterials with hyperbolic dispersion have also been proposed to achieve negative refraction and planar focusing; however, because of the dispersion characteristics of these media, focusing is always partial, as waves with large transverse wave number typically remain unfocused [16,17]. Here, we explore a different route to imaging beyond the limitations of classical optics, based on parity-time (PT) symmetric systems that can realize loss-immune, transversely invariant lenses [18], having the imaging properties of absolute optical instruments, without some of the limitations of existing metamaterial designs.

II. ABERRATION-FREE IMAGING AND PARITY-TIME SYMMETRY

Consider again the case of optical imaging by a plane mirror, sketched in Fig. 1(a). As mentioned above, an ideal mirror produces aberration-free *virtual* images of a *real* 3D object space. Our goal is to devise an optical system that realizes similar imaging properties, but in which both object and image spaces are real. As a first step, imagine going "through the looking glass" and assume that the virtual rays [red dashed arrows in Fig. 1(a)] beyond the mirror are real. In this scenario, we see that the imaging process is supported by a backward phase and power flow with respect to the positive z axis. Interestingly, we show in the following that such phase and power flow distributions are actually attainable in a nonlocal PT-symmetric system, hence opening the possibility of realizing the equivalent of aberration-free volumetric imaging by a mirror, but with a real image space.

To make our discussion as general as possible, we start by considering the fundamental conditions to realize ideal imaging of a 3D region of space, and we then derive—from first principles—the specific requirements that a structure should fulfill to implement this functionality. In analogy with the scattering response of a DNG lens, the scattering matrix of a generic two-port, linear, time-invariant system that performs ideal imaging should have, for any impinging propagating plane wave, the general form

$$S = \begin{pmatrix} 0 & e^{-i\beta d} \\ e^{-i\beta d} & S_{22} \end{pmatrix}, \tag{1}$$

which implies that (a) the structure should be reflectionless (i.e., impedance matched), at least from the input side, whereas, for now, we let S_{22} be an arbitrary complex quantity; (b) the structure should "rewind" the phase of waves propagating through a distance d with wave number $\beta = k_0 \cos\theta$, where k_0 is the free-space wave number and θ is the incidence angle [we assume a time-harmonic convention $e^{-i\omega t}$]; (c) the appropriate phase advance should be realized for any angle of incidence, and for any source position, implying that the structure should be transversely invariant. It is also important to note that in Eq. (1), we assumed reciprocity but not necessarily passivity; namely, the S matrix may be nonunitary.

In the special case $S_{22} = 0$ (which implies loss-free response), the scattering response in Eq. (1) can be implemented using an isotropic slab with refractive index $n = -1$, which realizes impedance matching and negative phase velocity for any angle [7,8]. Given the challenges associated with realizing such ideal DNG metamaterial response, we explore whether other structures can implement Eq. (1) without requiring magnetic or negative-index media. We consider a structure composed of two generic elements separated by a free-space region of length d, as sketched in Fig. 1(b), a design appealing for several reasons, as will become clear in the following. By using a transfer-matrix formalism applied to the considered structure (Appendix A), it is possible to derive the general requirements on the left and right elements to implement the desired S matrix. In particular, we perform an

eigendecomposition of the transfer matrix T corresponding to Eq. (1) and identify the different blocks of this expansion as different elements of the structure. By further requiring that these elements are symmetric and reciprocal, we find that, in order for the system of Fig. 1(b) to realize ideal imaging, the transfer matrices of the left and right blocks need to have the general form

$$T_L = T_R^{-1} = \begin{pmatrix} \frac{1}{2c} & \frac{Z_0}{2}\left(\frac{1\mp 2c}{c}\right) \\ \frac{1}{2Z_0}\left(\frac{1\pm 2c}{c}\right) & \frac{1}{2c} \end{pmatrix}, \tag{2}$$

where Z_0 is the wave impedance in free space, which depends on incidence angle and polarization, and c is an arbitrary complex quantity. In addition, the requirements of symmetry and reciprocity impose $S_{22} = \mp\,(1 - e^{-2i\beta d})/c$, which implies that the scattering matrix of the overall system, given by Eq. (1), is generally nonunitary, as energy gets absorbed and/or emitted by the structure.

As a relevant example, if we choose $c = 1/2$ and the upper sign in Eq. (2), the transfer matrices for the left and right elements of the system in Fig. 1(b) become

$$T_L = \begin{pmatrix} 1 & 0 \\ \frac{1}{Z_0/2} & 1 \end{pmatrix}, \qquad T_R = \begin{pmatrix} 1 & 0 \\ -\frac{1}{Z_0/2} & 1 \end{pmatrix}. \tag{3}$$

Given their symmetry, these transfer matrices can be realized by a pair of shunt-impedance sheets, or ultrathin metasurfaces, which corresponds to the structure originally considered in Ref. [18]. In particular, the left element of the pair is passive with positive resistance $R_L = +Z_0/2$, whereas the right element is active with negative resistance $R_R = -Z_0/2$. In other words, this system is composed of a parity-time symmetric pair of metasurface elements; i.e., it is invariant under reflection of time and space. By duality, choosing the opposite sign in Eq. (2) and $c = 1/2$, the same scattering response is obtained with a pair of series-impedance sheets. More in general, the S matrix (1) for ideal imaging can be realized with a pair of structures in free space having transfer matrices given by Eq. (2)—one acting as the time-reversed counterpart of the other—separated by a distance d. Note that the value of the parameter c and the sign choice in Eq. (2) only affect the value of S_{22} in Eq. (1), whereas the phase advance and the unidirectional reflectionless response are ensured by the general form of the matrices in Eq. (2). These results confirm and generalize the findings in Ref. [18], showing that PT-symmetric metasurface pairs represent an ideal platform to explore the possibility of aberration-free volumetric imaging.

III. NONLOCAL PT-SYMMETRIC METASURFACES

In a different context, the concept of PT-symmetry has recently sparked much interest in both quantum and classical physics [18–27]. Classical optics provides a particularly fertile ground for these concepts, as PT-symmetric systems can be readily realized with spatially balanced distributions of gain and loss. The unusual properties of PT-symmetric structures have been shown to enable loss compensation, exotic scattering effects, unidirectional invisibility, and many other interesting features that go beyond the limits of conventional passive systems [22–27]. In Ref. [18], it was realized that, if two ultrathin parallel metasurfaces are designed to have impedance $R = \pm Z_0/2$ as in Eq. (3), for a certain incidence angle and polarization, the pair indeed becomes unidirectional reflectionless, and it supports negative phase and energy velocity, flowing backward from the active to the passive metasurface, hence implementing a scattering response consistent with Eq. (1) for the specific plane wave of interest. In order to use this feature to image a point source, in Ref. [18] a transversely inhomogeneous impedance profile of the two PT-symmetric surfaces was considered. This scenario unfortunately works only for a specific object point—and it operates somewhat analogous to a hologram—with a response inevitably distorted if the source is moved or changed.

In order to achieve aberration-free imaging, on the contrary, an all-angle negative refraction response is required, implying that the condition $R = \pm Z_0/2$ on the surface impedance needs to be fulfilled for any angle of incidence. This is challenging because the wave impedance of obliquely incident plane waves is naturally dispersive with the incidence angle θ, i.e., $Z_0(\theta) = \eta_0 \cos(\theta)$ for TM polarization (magnetic field orthogonal to the incidence plane). A PT-symmetric metasurface pair can therefore achieve all-angle negative refraction only if the metasurface impedance becomes spatially dispersive (i.e., nonlocal [28]), with a specifically prescribed angle dependence that compensates the natural angular dispersion of the wave impedance.

Based on these considerations, our goal is to design a PT-symmetric metasurface pair that implements this required spatially dispersive response. If the left element has transfer matrix exactly equal to Eq. (2) for any angle of incidence, its corresponding scattering matrix becomes

$$S_L = c\begin{pmatrix} \mp 1 & +1 \\ +1 & \mp 1 \end{pmatrix}, \tag{4}$$

independent of the angle of incidence. Interestingly, as discussed in Appendixes A and B, this scattering matrix represents the response of an omnidirectional coherent perfect absorber (CPA), namely, a device that absorbs the complete angular spectrum of plane waves when illuminated at the same time from both sides with waves satisfying a given phase relation (which generalizes the recently proposed concept of coherent perfect absorber [28,30,31] to all-angle operation). Different from a conventional absorber (such as, e.g., Refs. [32–34]), a CPA only provides full

absorption when it is bilaterally illuminated, whereas its reflection and transmission are nonzero when excited from a single side. As shown in Appendix B, when a symmetric structure is bilaterally illuminated with waves having equal amplitude and relative phase difference $\Delta\phi$, the omnidirectional CPA operation requires that the reflection R and transmission T coefficients respect the condition

$$R - T\, e^{i\Delta\phi} = 0 \quad \forall\ \theta, \tag{5}$$

where R and T do not depend on the angle of incidence. It follows that the scattering matrix of the left element, given by Eq. (4), indeed represents an omnidirectional CPA with $\Delta\phi = 0, \pi, R = \mp\, c$ and $T = c$, achieving perfect absorption for symmetric or antisymmetric illumination.

In Fig. 1(b), we show a sketch of the complete "PT-symmetric lens," with the expected ray trajectories under point-source illumination. As qualitatively seen in this ray picture, the lens functionality is indeed based on the fact that the left passive element operates as a CPA, whereas the right active element, which is the time-reversed version of the CPA, acts as a coherently emitting system for all excitation angles, amplifying the incoming signals and reproducing them symmetrically and coherently on both sides. We first focus on the design of the CPA, considering that the active element will be obtained by time reversing the CPA response.

In an implementation based on zero-thickness metasurfaces, as in Ref. [18], the condition of angle independency of the scattering parameters in Eq. (4) indeed requires the impedance to become angle dependent (spatially dispersive), in order to compensate the angular dispersion of the incident wave impedance. Here, in order to realize this response, we consider structures with small but finite thickness, which allow engineering the required scattering matrix (4) with the desired nonlocal response. In particular, we consider transversely homogeneous thin multilayered planar slabs, in which each layer has a purely local response, but multiple reflections enable engineering the desired angular reflection and transmission spectra, with an approach analogous to the one recently employed to realize computational metastructures [35]. In other words, we obtain an effective nonlocal response by tailoring the longitudinal inhomogeneity of the thin stack, so the multilayer is seen by the incident wave as a homogeneous spatially dispersive metasurface. This represents a general and powerful approach to implement a desired nonlocal response, which is of great interest even beyond the scope of the present work.

As an example, for bilateral excitation from TM-polarized sources with $\Delta\phi = \pi$, we chose to design a multilayered lossy structure having $R = -0.5$ and $T = 0.5$, consistent with Eqs. (4) and (5). This target design represents a strongly nonlinear inverse-design problem, with no analytical solution even for a few layers, which is best tackled by relying on numerical optimization. Following this approach, as detailed in Ref. [36], we designed a thin symmetric stack of ten lossy layers that realizes the desired reflection and transmission coefficients, approximately constant as a function of angle. It should be stressed here that we considered no magnetic material, or other unconventional material properties in this design [36], making the fabrication of the structure feasible and practically appealing. We also note that, while the level of gain considered in the proposed design [36] may be difficult to achieve at optical frequencies, by further optimizing the structure, we expect to be able to relax these requirements. In addition, larger gain or amplification can readily be achieved at radiofrequencies and for acoustic waves (as shown, e.g., in Ref. [26]), areas in which we believe that our proposed concept may find very fertile ground. As discussed in Ref. [36], we have also verified that the designed structure is moderately robust to variations of geometrical and material properties, and it can be further simplified without seriously affecting its performance. Figures 2(a) and 2(b) show the calculated reflection and transmission angular spectra, while Figs. 2(c) and 2(d) show the field distributions [37] for different point-source illuminations (time-harmonic animations are provided in Ref. [36]). Despite being transversely homogeneous, the designed structure indeed operates as an omnidirectional CPA, absorbing the impinging radiation only when illuminated from both sides with waves having the correct phase relation. Because of the translational symmetry, this response is independent of the source position and angular spectrum.

A full PT-symmetric lens can now be obtained by pairing the designed passive CPA with its time-reversed counterpart, as sketched in Fig. 1(b). This active element is obtained by conjugating the permittivity distribution obtained in the CPA design, such that $\varepsilon(\boldsymbol{r}) = \varepsilon^*(-\boldsymbol{r})$, where $\mathbf{r}$ is the position vector from the center of the PT-symmetric lens. The scattering matrix of the complete system is indeed equal to Eq. (1) [with $S_{22} = -2(e^{-2i\beta d} - 1)$], and the designed PT-symmetric lens is therefore unidirectional reflectionless when illuminated from the CPA side, irrespective of the impinging wave front, and the transmitted plane waves exhibit a phase advance $\Phi = -\beta d$. These properties are consistent with the findings in Ref. [18] for a pair of ultrathin PT-symmetric metasurfaces but with the fundamental difference that here they are achieved for any angle of incidence, thanks to the implemented nonlocal response, and they are independent of the thickness L of the active and passive elements. The numerically computed field distribution in Fig. 3 confirms that, under point-source illumination from the left side, the proposed PT-symmetric lens indeed performs, at steady state, as an impedance-matched all-angle negative refraction slab, with negative phase and energy velocity, flowing from the active to the passive element (a time-harmonic animation is shown in Ref. [36]), consistent with the ray picture in Fig. 1(b). We stress that this functionality works independent of the distance between passive and active elements, and simply assumes free space in

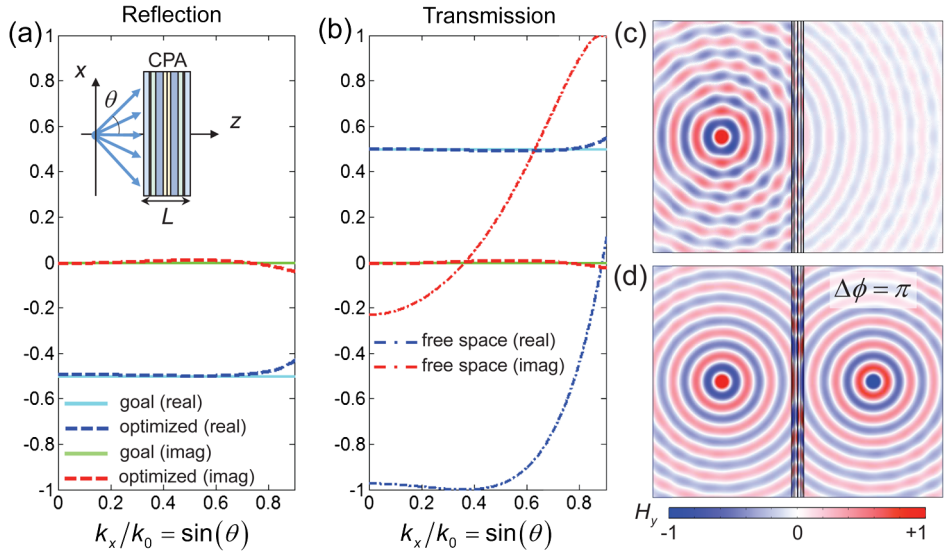

FIG. 2. Omnidirectional CPA based on a thin multilayered planar slab [inset of panel (a)]. (a) Reflection and (b) transmission coefficients, as a function of the normalized transverse wave number k_x/k_0, for the optimized structure (dashed lines: red, imaginary part; blue, real part), and goal functions $R = -0.5$ and $T = 0.5$ (solid lines: green, imaginary part; cyan, real part). The total length of the optimized CPA is only $L = 0.537\lambda_0$, where λ_0 is the free-space wavelength (details in Ref. [36]). For comparison, in panel (b), we also show the transmission coefficient (dot-dashed lines) of an equivalent free-space slab having the same length L, i.e., $T_{fs}(k_x) = \exp(i\sqrt{k_0^2 - k_x^2}L)$, which highlights the challenge of realizing angle-independent scattering parameters. (c,d) Magnetic-field distribution (time snapshot) of the designed omnidirectional CPA under illumination from (a) a single TM-polarized point source and (d) two symmetrically located point sources with phase difference $\Delta\phi = \pi$ (animations in Ref. [36]).

between the two structures. This represents the first example of all-angle negative refraction achieved in a loss-immune, metamaterial-free, linear, and transversely invariant system, with important implications for imaging, as we discuss in the following. In contrast with DNG lenses, in which material absorption is strongly detrimental for the performance of the device (Appendix C), here losses are at the very basis of the lensing mechanism, hence demonstrating the power of PT-symmetry concepts to go beyond the limitations of passive metamaterial structures.

We stress here that Figs. 1(b) and 3 refer to the steady-state response of the system, consistent with our scattering

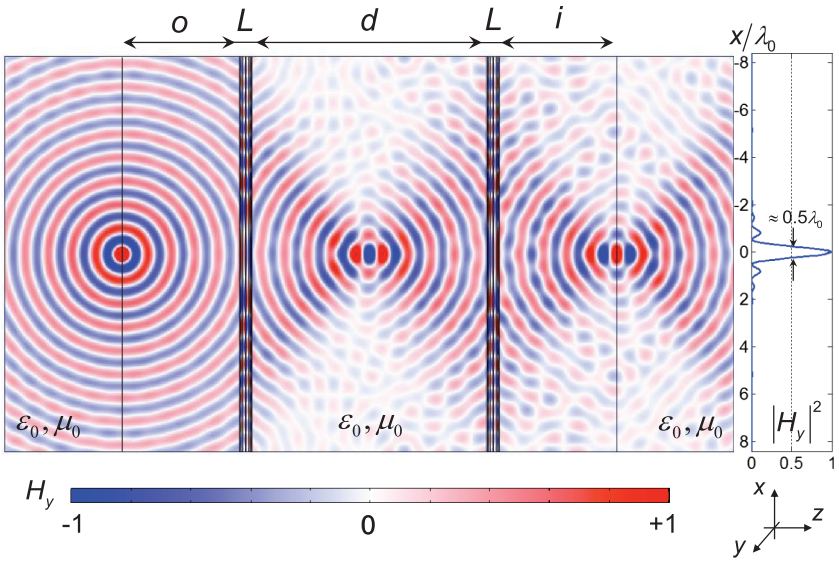

FIG. 3. Magnetic-field distribution (time snapshot) of the proposed PT-symmetric lens at steady state, under TM-polarized point-source illumination on the left side (animation in Ref. [36]). The lens is homogeneous along the transverse x direction. The inset on the right shows the field intensity on the focal plane (at distance i from the active element), demonstrating transverse resolution very close to the diffraction limit.

matrix analysis in Sec. II. At steady state, the object and image planes are decoupled, as the left element completely absorbs the input energy, and the right element creates an image identical to and in sync with the object plane while feeding the same image back into the absorbing element. This balanced bilateral excitation is required by the CPA to fully absorb the impinging signal. When the system is initially excited only from the left side, however, there is not a signal from the right side of the coherent absorber; therefore, in the transient regime, the system partially reflects and transmits the incident illumination. As a result, some of the input energy reaches the right active element and is amplified by it. During this regime, the active element is able to "synchronize" with the input signal, and—at steady state—it will converge to equilibrium, with the response shown in Fig. 3. Should the input signal change in amplitude and/or phase at some point in time, the CPA functionality will not instantaneously work any longer, allowing a portion of the new signal to trickle to the active side and reach a new steady state. In other words, any *information* about the object to be imaged is transmitted during the transient regime when the source is initially switched on, or when it undergoes any modification, and the system uses this transient to lock on an exact replica of the object plane. The specific temporal dynamics of the PT-symmetric system in the transient regime depend on the frequency dispersion of the involved material properties and therefore on the specific implementation of the passive and active elements of the structure. Although the specific frequency dispersion of the elements is not relevant once the system has reached a steady state, it is crucial to know whether the system can be made stable so that the steady-state regime can indeed be reached. To address this relevant point, in Ref. [36], we extensively discuss the transient response of an example of a dispersive PT-symmetric lens, and we assess its overall stability. In particular, we show that the system can be made unconditionally stable by suitably choosing the frequency dispersion of the passive and active metasurfaces. These results, and the transient animations in Ref. [36], fully clarify how the response of the system evolves toward a steady state and how the image information propagates through the system in the transient, confirming the above qualitative discussion.

We believe that the nontrivial and seemingly counterintuitive mechanism of the proposed device, and its unusual, yet stable, temporal dynamics, represents an exciting example of the kind of anomalous responses that can be achieved by combining loss and gain in PT-symmetric systems.

IV. IMAGING PROPERTIES OF PT-SYMMETRIC LENSES

As shown in Fig. 1(b), and confirmed in Fig. 3, light rays emanating from a point source at distance o from the PT-symmetric lens are again focused at two distinct points, creating two real images of the source: the first in the central region of the lens, at a distance o from the passive element, and the second outside the lens, at a distance $i = d - o$ from the active element. If the distance o is larger than d, then the images become "virtual," in the sense that the rays will diverge from the active element (an example of this response, with associated animation, is reported in Ref. [36]).

This imaging response is similar to that of other systems based on negative refraction, but with significant differences. In fact, different from DNG and photonic crystal lenses, the first image can indeed be accessed for imaging purposes, as it is formed in free space; and different from phase-conjugating devices, the efficiency of the proposed PT-symmetric lens may be significantly larger since it is based on a linear scattering process. Another interesting feature of the proposed PT-symmetric lens is that the relative phase of the central image can be controlled by the parameter $\Delta\phi$ of the CPA structure (it can be seen in Fig. 3 that the central image has a phase difference of $\Delta\phi = \pi$ with respect to the point source), an intriguing possibility for wave manipulation [38]. As expected, the images produced by the PT-symmetric lens have diffraction-limited transverse resolution because evanescent waves are not time reversible; therefore, they do not contribute to the operation of a PT-symmetric system. However, as seen in the inset of Fig. 3, the focus spot has transverse width $\approx 0.5\lambda_0$, where λ_0 is the free-space wavelength, which demonstrates that the designed PT-symmetric lens is close to ideal from the point of view of geometrical optics. Moreover, as seen in Fig. 3, the PT-symmetric lens offers good resolution in both transverse and longitudinal directions, which is different from the response of an ideal lossless DNG lens, in which subdiffractive transverse resolution inevitably comes at the expense of reduced longitudinal resolution because of the strong resonant fields induced on the exit interface of the lens [10,11].

The imaging properties of the proposed PT-symmetric lens are fundamentally different from any system of conventional lenses (i.e., based on conventional refraction). Remarkably, since the proposed setup is planar and transversely invariant, an ensemble of sources can, in principle, be moved laterally in the object space without any distortion or aberration. Instead, while conventional lenses can be made planar, e.g., graded-refractive-index lenses, or, more recently, metasurface lenses [40,41], they can never be transversely homogeneous because they need to compensate, point by point, the phase difference of the light rays emerging from the source (conversely, PT-symmetric lenses, or DNG lenses, automatically "rewind" the phase of the rays due to a negative phase velocity). In particular, conventional lenses have a definite optical axis, corresponding to the axis of rotational symmetry, and a definite focal distance f that depends on the lens geometry. Conventional lens imaging is essentially based on the "thin-lens formula," $1/i + 1/o = 1/f$ [1], relating the position i of the image to the position o of the source, through the focal distance. Instead, because of

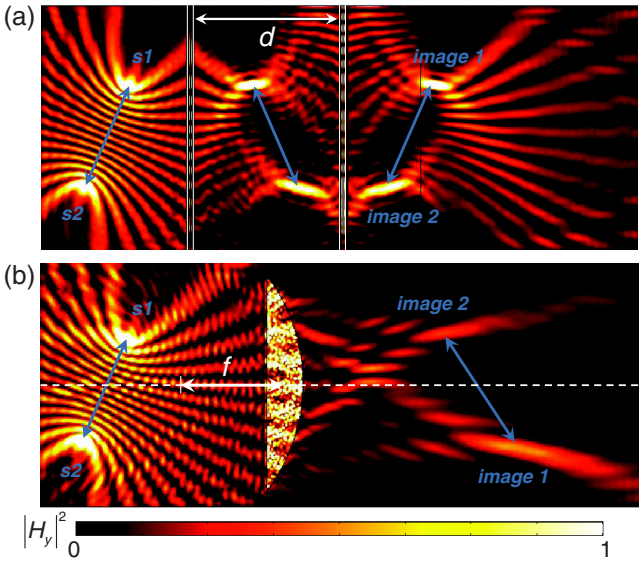

FIG. 4. Comparison between the field-intensity distribution of (a) the proposed PT-symmetric lens, with length d, and (b) a conventional spherical dielectric lens (refractive index $n = 2.5$) with focal length f, under illumination from two point sources s1 and s2 located on different transverse planes. The spherical lens is coated, on the planar face, with a quarter-wavelength antireflection coating, having refractive index $n_{ar} = \sqrt{n} = 1.58$. The blue arrows indicate the relative position of sources and images, highlighting the different imaging properties of the two lenses. The proposed PT-symmetric lens may realize volume-to-volume imaging.

transverse invariance, PT-symmetric lenses do not have an optical axis, are inherently afocal, and follow a different imaging rule, $i = d - o$, which implies that the position of the external image can be controlled by varying the distance d between active and passive elements of the lens. In order to visually appreciate these different imaging properties, in Fig. 4 we compare the response of the designed PT-symmetric lens [Fig. 4(a)] with that of a conventional spherical lens [Fig. 4(b)] under illumination from two point sources. Notably, since the two sources are located on different transverse planes, the spherical lens inevitably distorts the relative distance between their images, according to the thin-lens formula; conversely, because of its afocal nature, the PT-symmetric lens always preserves relative distances and angles between points (as indicated by the blue arrows in Fig. 4), which is indeed one of the main characteristics of planar absolute optical instruments. Moreover, as seen in Fig. 4, the image points produced by the PT-symmetric lens are significantly sharper and more intense, whereas some degree of distortion or aberration (as well as reflection) is always expected for conventional lenses [1–3].

The level of residual aberrations of the proposed PT-symmetric lens depends on the level at which the desired properties are implemented [namely, it depends on how well the left and right elements implement the transfer matrices given by Eq. (2)]. However, it is important to stress that such aberrations are not inherent to the imaging process, as in the case of conventional refractive optics; in principle, they may be made arbitrarily small, as shown by our theoretical analysis in Sec. II and Appendix A. This is an important point, as it indicates that there is no fundamental lower bound on the level of aberration in an imaging system based on PT-symmetry. More generally, the intriguing properties of PT-symmetric lenses may lead to the realization of aberration-free imaging devices, which may produce perfectly focused 3D images of a large region of space (volume-to-volume imaging, rather than plane-to-plane imaging as in conventional refractive optics), of significant interest for several practical applications.

V. SUMMARY

In conclusion, in this paper, we have demonstrated that suitably designed PT-symmetric systems, combined with a tailored nonlocal response, allow one to realize loss-immune, metamaterial-free, linear, transversely invariant, aberration-free lenses, which implement the imaging properties of planar absolute optical instruments without some of the limitations of existing metamaterial lenses. In particular, the negative phase and power-flow distributions support an imaging process analogous to the one of an ideal plane mirror, as seen in Fig. 1, but with a real image space. This represents an interesting parallel between PT-symmetric lens imaging, which is based on space-time mirror symmetry, and conventional mirror imaging. It should also be noted that, since the proposed PT-symmetric lens is afocal, it cannot perform image magnification, which may be a useful feature in many applications. To circumvent this limitation, we are currently exploring PT-inspired cylindrical lenses that may allow one to realize a general platform for imaging and wave manipulation. While a proof-of-concept realization of these ideas may be readily envisioned at microwave or acoustic frequencies using suitably designed stacks of passive and active metasurfaces, at optical frequencies the use of parametric gain may be explored to realize low-noise, linear gain elements. We also would like to mention that, for the frequency of interest, the specific implementation of the amplification process is not relevant at steady state. However, when dealing with the evolution and temporal dynamics of the system in the transient regime, one needs to consider the specific dispersion of the active elements, as well as the possible nonlinearities associated with the practical implementation of the amplification process. This is also associated with stability considerations due to the presence of active elements. In fact, the stability of the overall system needs to be properly assessed in order to ensure that, in the presence of noise and of scattering from other objects around the system, and for an arbitrary temporal evolution of the excitation, the system will not exhibit self-oscillations and instabilities. This is indeed possible, as we have shown in Ref. [36] for an example of a

dispersive PT-symmetric lens. By properly tailoring the frequency dispersion of the passive and active elements, in fact, the system can be made unconditionally stable for any temporal excitation, and for any distance between the metasurfaces composing the lens, which confirms the feasibility of the proposed structure to robustly realize negative refraction and unconventional imaging functionalities.

We believe that our results highlight the exciting potential of PT-symmetric spatially dispersive metasurfaces for volumetric imaging. The general concepts put forward in this paper may find application for different kinds of waves, and in various frequency regimes (not limited to optical frequencies), opening uncharted directions in the field of imaging.

ACKNOWLEDGMENTS

This work was supported by the Air Force Office of Scientific Research with Grant No. FA9550-13-1-0204, the Office of Naval Research with Grant No. N00014-15-1-2685, the Welch Foundation with Grant No. F-1802, and the Simons Foundation. C. A. V. was partially supported by the Academy of Finland under Project No. 13260996.

APPENDIX A: DERIVATION OF PT-SYMMETRY CONDITIONS FOR IDEAL ABERRATION-FREE IMAGING

Equation (1) represents the scattering matrix of a generic system that performs ideal aberration-free imaging. In order to design a structure that realizes this scattering response, it is useful to use a transfer-matrix formalism, in which the cascade of different blocks can be represented as the cascade (matrix product) of their transfer matrices. The transfer matrix corresponding to Eq. (1) can readily be obtained (see, e.g., Ref. [42]):

$$T = \begin{pmatrix} \cos(\beta d) - \frac{1}{2} S_{22} e^{i\beta d} & +iZ_0 \sin(\beta d) + \frac{1}{2} Z_0 S_{22} e^{i\beta d} \\ +i \sin(\beta d)/Z_0 - \frac{1}{2Z_0} S_{22} e^{i\beta d} & \cos(\beta d) - \frac{1}{2} S_{22} e^{i\beta d} \end{pmatrix}, \tag{A1}$$

which has a unitary determinant and, if $S_{22} = 0$, it becomes equal to the transfer matrix of a transmission line of length d and negative phase velocity $v_p = \omega/\beta = -c_0/\cos\theta$ (where c_0 is the speed of light in vacuum, and θ is the incidence angle), exactly the opposite compared to a free-space region of the same length.

Here, we implement Eq. (A1) as the cascade of three blocks, as shown in Fig. 5: two elements with transfer matrices T_L and T_R, separated by an air region of length d modeled as a transmission line with transfer matrix

$$T_{\text{line}} = \begin{pmatrix} \cos(\beta d) & -iZ_0 \sin(\beta d) \\ -i \sin(\beta d)/Z_0 & \cos(\beta d) \end{pmatrix}. \tag{A2}$$

Our goal is therefore to determine T_L and T_R such that

$$T = T_L T_{\text{line}} T_R. \tag{A3}$$

To solve this problem, we perform an eigendecomposition of the square matrices T and T_{line}, which allows us to write them in terms of their eigenvalues and eigenvectors as

$$\begin{aligned} T &= V \Lambda V^{-1} \\ T_{\text{line}} &= V_{\text{line}} \Lambda_{\text{line}} V_{\text{line}}^{-1}, \end{aligned} \tag{A4}$$

where the columns of V and V_{line} are the eigenvectors of the transfer matrices, whereas Λ and Λ_{line} are diagonal matrices whose elements are the corresponding eigenvalues. With this decomposition, we can write Eq. (A3) as

$$V \Lambda V^{-1} = T_L (V_{\text{line}} \Lambda_{\text{line}} V_{\text{line}}^{-1}) T_R. \tag{A5}$$

Interestingly, the matrices T and T_{line} have the same eigenvalues; therefore,

$$\Lambda = \Lambda_{\text{line}} = \begin{pmatrix} e^{i\beta d} & 0 \\ 0 & e^{-i\beta d} \end{pmatrix}. \tag{A6}$$

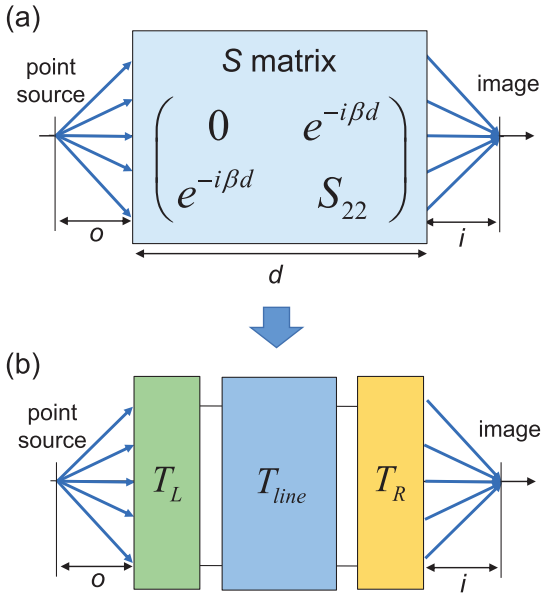

FIG. 5. (a) Generic structure that realizes ideal aberration-free imaging, according to the scattering matrix S in Eq. (1), and (b) desired implementation composed of the cascade of three blocks, characterized by transfer matrices T_L, T_{line}, and T_R.

(Note that $\Lambda = \Lambda_{\text{line}}$ only if we assume that the corresponding structures have identical length d; however, if the structures have different lengths, say d and d_l, we can write

$$\begin{aligned}\Lambda_{\text{line}} &= \text{diag}(e^{\pm i\beta d_l}) = \text{diag}(e^{\pm i\beta(d_l-d)/2}) \\ &\cdot \text{diag}(e^{\pm i\beta d}) \cdot \text{diag}(e^{\pm i\beta(d_l-d)/2}) \\ &= \text{diag}(e^{\pm i\beta(d_l-d)/2}) \cdot \Lambda \cdot \text{diag}(e^{\pm i\beta(d_l-d)/2}) \end{aligned} \quad \text{(A7)}$$

and the following derivation is only slightly modified.)

By applying Eq. (A6) to Eq. (A5), it follows that

$$\begin{aligned} V &= T_L\, V_{\text{line}} \\ V^{-1} &= V_{\text{line}}^{-1} T_R \end{aligned}, \quad \text{(A8)}$$

and, since V and V_{line} are known, we can find the transfer matrices of the left and right elements by simply inverting Eq. (A8):

$$\begin{aligned} T_L &= V\, V_{\text{line}}^{-1} \\ T_R &= V_{\text{line}} V^{-1} \end{aligned}. \quad \text{(A9)}$$

Note also that, since the inverse of a matrix product is anticommutative, the left and right transfer matrices are the inverse of each other, i.e.,

$$T_R = T_L^{-1}. \quad \text{(A10)}$$

Finally, we build the matrices V and V_{line} from the eigenvectors of the corresponding transfer matrices:

$$\begin{aligned} V_{\text{line}} &= \begin{pmatrix} a_l & b_l \\ \frac{a_l}{Z_0} & -\frac{b_l}{Z_0} \end{pmatrix}, \\ V &= \begin{pmatrix} a & b \\ a\,\frac{S_{22}\cos(\beta d)+i(-2+S_{22})\sin(\beta d)}{S_{22}Z_0\cos(\beta d)+i(2+S_{22})Z_0\sin(\beta d)} & \frac{b}{Z_0} \end{pmatrix}, \end{aligned} \quad \text{(A11)}$$

where a, b, a_l, $b_l \in \mathbb{C}$ are arbitrary nonzero complex constants (for any value of these constants, the columns of the matrices above represent eigenvectors of the corresponding transfer matrices). Equation (A11) can be substituted into Eq. (A9) to find the transfer matrices $T_L = T_R^{-1}$, whose general expression is not written here for the sake of brevity. The corresponding scattering matrix of the left element can be written as

$$S_L = \begin{pmatrix} \frac{2i}{S_{22}[i+\cot(\beta d)]} & -\frac{2bi}{b_l S_{22}[i+\cot(\beta d)]} \\ \frac{a_l}{a}\left(1+\frac{2i}{S_{22}[i+\cot(\beta d)]}\right) & -\frac{a_l b[i(2+S_{22})+S_{22}\cot(\beta d)]}{a b_l S_{22}[i+\cot(\beta d)]} \end{pmatrix}, \quad \text{(A12)}$$

which represents the most general form of S_L to realize a system, as in Fig. 5, with the overall S matrix given by Eq. (1), namely, a system that performs ideal imaging. Equation (A12) represents a structure that is generally nonreciprocal and nonsymmetric and that can absorb or emit energy (the scattering matrix is nonunitary). However, the structure can easily be made reciprocal by imposing

$$S_{22} = -2i\frac{ab + a_l b_l}{a_l b_l[i + \cot(\beta d)]}. \quad \text{(A13)}$$

If we further require the left element to be symmetric, namely, with identical reflection coefficient from both sides, we obtain the following condition:

$$b = \pm b_l, \quad \text{(A14)}$$

which should hold for any a, a_l, b, $b_l \in \mathbb{C}$. If, for example, we choose the plus sign in Eq. (A14), and substitute it in Eq. (A12) together with the reciprocity condition (A13), we obtain

$$S_L = \begin{pmatrix} -c & c \\ c & -c \end{pmatrix}, \quad \text{(A15)}$$

where we introduced a new complex constant $c = a_l/(a + a_l)$. With these assumptions, the corresponding transfer matrices become

$$T_L = T_R^{-1} = \begin{pmatrix} \frac{1}{2c} & \frac{Z_0}{2}\left(\frac{1-2c}{c}\right) \\ \frac{1}{2Z_0}\left(\frac{1+2c}{c}\right) & \frac{1}{2c} \end{pmatrix}, \quad \text{(A16)}$$

which can be implemented with a suitably designed symmetric T or Π circuit network [42]. In particular, if we choose $c = 1/2$, the reciprocity condition for S_L, given by Eq. (A13), simplifies to $S_{22} = -2(1 - e^{-2i\beta d})$, and the transfer matrices become

$$T_L = \begin{pmatrix} 1 & 0 \\ \frac{1}{Z_0/2} & 1 \end{pmatrix}, \qquad T_R = \begin{pmatrix} 1 & 0 \\ -\frac{1}{Z_0/2} & 1 \end{pmatrix}, \quad \text{(A17)}$$

which represent a parity-time symmetric pair of shunt-impedance sheets, or metasurfaces, with impedance value $R = \pm Z_0/2$. Equation (A17) corresponds to Eq. (3) above.

Instead, if we choose the minus sign in the symmetry condition (A14), the scattering matrix of the left element becomes

$$S_L = \begin{pmatrix} c & c \\ c & c \end{pmatrix}, \quad \text{(A18)}$$

where now $c = a_l/(a - a_l)$, and the corresponding transfer matrices are found to be

$$T_L = T_R^{-1} = \begin{pmatrix} \frac{1}{2c} & \frac{Z_0}{2}\left(\frac{1+2c}{c}\right) \\ \frac{1}{2Z_0}\left(\frac{1-2c}{c}\right) & \frac{1}{2c} \end{pmatrix}. \quad \text{(A19)}$$

Equations (A16) and (A19) together correspond to Eq. (2), and Eqs. (A15) and (A18) correspond to Eq. (4). Again, if we choose $c = 1/2$ in Eq. (A19), the reciprocity condition for S_L, given by Eq. (A13), simplifies to $S_{22} = +2(1 - e^{-2i\beta d})$, and the transfer matrices become

$$T_L = \begin{pmatrix} 1 & 2Z_0 \\ 0 & 1 \end{pmatrix}, \qquad T_R = \begin{pmatrix} 1 & -2Z_0 \\ 0 & 1 \end{pmatrix}, \quad \text{(A20)}$$

which are exactly the dual of Eqs. (A17) and represent a pair of series-impedance sheets of value $R = \pm 2Z_0$.

As mentioned in the main text, and further discussed in Appendix B, both Eqs. (A15) and (A18) represent the scattering matrix of a symmetric and reciprocal coherent perfect absorber (CPA) (however, all this discussion can readily be extended, in the most general scenario, to CPAs that are both nonsymmetric and nonreciprocal). In particular, the fact that symmetry determines two possible forms for the scattering matrix of the left element, i.e., Eqs. (A15) or (A18), is consistent with the fact that, in the case of a symmetric structure, ideal CPA operation can be achieved *only* for symmetric or antisymmetric excitation, corresponding to either Eq. (A15) or Eq. (A18) according to whether the excitation is TE or TM polarized, as discussed in Appendix B.

In summary, Eqs. (A15) and (A18) give the scattering matrix of the left element of the system in Fig. 5(b), assuming this element is reciprocal and symmetric. Interestingly, it can easily be verified that the right element of the system is instead characterized by a nonfinite S matrix, consistent with the fact that the right element is an active, coherently emitting structure (i.e., the time-reversed counterpart of a CPA). Nevertheless, the scattering matrix of the entire system is finite and is given by

$$S = \begin{pmatrix} 0 & e^{-i\beta d} \\ e^{-i\beta d} & \mp\frac{1-e^{-2i\beta d}}{c} \end{pmatrix}, \quad \text{(A21)}$$

in which the minus (plus) sign corresponds to the plus (minus) sign in Eq. (A14), and c is again a generic complex constant. Equation (A21) is indeed of the form of Eq. (1). As is typical of PT-symmetric systems, the response of the proposed structure is strongly asymmetric, with no reflection when excited from the left side, whereas reflections are expected when the system is illuminated from the right. Instead, the transmission is identical from both sides since the structure is reciprocal. Since the system is fully linear, if there are sources on the right of the device, the final image will be a superposition of the desired image and the response to the sources on the right of the device.

APPENDIX B: OMNIDIRECTIONAL COHERENT PERFECT ABSORBERS

The scattering-matrix formalism allows us to obtain the vector of outgoing waves b at the different "ports" of a structure from the vector of input waves a through the scattering matrix of the structure. For a generic slab, illuminated from both sides with waves having equal amplitude $|a| \neq 0$ and relative phase difference $\Delta\phi$, as illustrated in Fig. 6, the scattering-parameter system of equations becomes

$$\begin{pmatrix} b_1 \\ b_2 \end{pmatrix} = \begin{pmatrix} S_{11} & S_{12} \\ S_{21} & S_{22} \end{pmatrix} \begin{pmatrix} a \\ a\, e^{i\Delta\phi} \end{pmatrix}. \quad \text{(B1)}$$

CPA operation implies that the outgoing waves need to completely vanish, i.e., $b_1 = b_2 = 0$. The trivial solution with all scattering parameters equal to zero (vanishing reflection and transmission coefficients), however, needs to be excluded since it corresponds to a conventional perfect absorber, in which perfect absorption under unilateral excitation is achieved independently of what happens at the other port (which can indeed be substituted by a short circuit, as in grounded absorbing slabs). Instead, in a CPA, perfect absorption is obtained as the result of interference between reflected and transmitted waves under bilateral excitation. Therefore, the conditions for CPA operation read

$$\begin{aligned} S_{11} + S_{12}e^{i\Delta\phi} &= 0, \\ S_{21} + S_{22}e^{i\Delta\phi} &= 0. \end{aligned} \quad \text{(B2)}$$

If we assume that the structure is reciprocal, i.e., $S_{12} = S_{21} = T$, and symmetric, i.e., $S_{11} = S_{22} = R$, as in the case considered in the main text and in Appendix A, Eqs. (B2) become

$$\begin{aligned} R + Te^{i\Delta\phi} &= 0, \\ T + Re^{i\Delta\phi} &= 0, \end{aligned} \quad \text{(B3)}$$

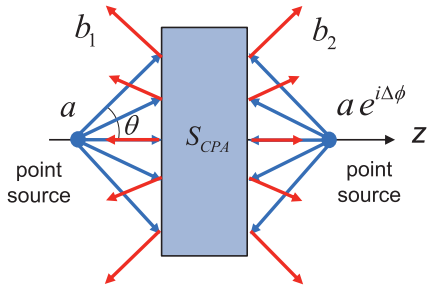

FIG. 6. Sketch of a generic slab described by a two-port scattering matrix S_{CPA}, with input incoming waves a and $a\,e^{i\Delta\phi}$ (blue arrows), and output outgoing waves b_1 and b_2 (red arrows), consistent with Eq. (B1). For CPA operation, the outgoing waves need to completely vanish, as a result of interference and dissipation in the structure.

which can be simultaneously true only if $\Delta\phi = 0, \pi, 2\pi, ...$ In other words, because of the mirror symmetry of the structure, CPA operation can be achieved only for symmetric or antisymmetric excitation, as mentioned in Appendix A and discussed in Ref. [30]. Instead, nonsymmetric structures can realize, in principle, coherent absorption for arbitrary phase difference $\Delta\phi$, with interesting implications for imaging and wave manipulations, as we will discuss in a future paper. It is also important to note that the quantities a_i and b_i are typically defined as voltage waves in an equivalent transmission line, which models the longitudinal wave propagation in the considered system (see, e.g., Ref. [42]). In particular, the voltage corresponds to the transverse component of the electric field of the propagating wave. Therefore, if the sources illuminating the structure in Fig. 6 are TE polarized (transverse out-of-plane electric field), the condition for CPA operation directly follows from the above equations:

$$R + Te^{i\Delta\phi} = 0, \qquad \Delta\phi = 0, \pi. \tag{B4}$$

Instead, if the sources are defined in terms of a transverse magnetic field, which corresponds to the current in the equivalent transmission-line model, Eq. (B4) needs to be slightly modified to account for the minus sign in the definition of current waves propagating in the $-z$ direction [42]:

$$R - Te^{i\Delta\phi} = 0, \qquad \Delta\phi = 0, \pi. \tag{B5}$$

which corresponds to Eq. (4) for TM-polarized illumination. The sign difference in Eqs. (B4) and (B5) is consistent with the fact that, when a CPA structure is illuminated by antisymmetric TM-polarized sources (i.e., $\Delta\phi = \pi$), as in Fig. 2(d), the corresponding transverse electric fields (E_x component), impinging from the two sides, are actually in phase.

In light of this discussion, it is therefore clear that the left element of the structure in Fig. 5(b), whose scattering matrix is given by Eq. (A15) or (A18), is indeed a CPA structure with $|R| = |T| = c$. In particular, Eq. (A15) corresponds to the case of symmetric TE excitation [condition (B4) with $\Delta\phi = 0$, as considered in Ref. [18]] or the case of antisymmetric TM excitation [condition (B5) with $\Delta\phi = \pi$, as considered in the main text]. Conversely, Eq. (A18) corresponds to the case of antisymmetric TE excitation [condition (B4) with $\Delta\phi = \pi$] or the case of symmetric TM excitation [condition (B5) with $\Delta\phi = 0$].

From the physical standpoint, Eq. (B4), or (B5), indicates that the reflected wave from one side of the structure destructively interferes with the wave transmitted from the other side, such that the field is confined in an interference pattern within the CPA structure and gets completely absorbed, as discussed in Ref. [30]. In general, however, this effect occurs only at a specific incidence angle, or within a narrow angular range, as the reflection and transmission coefficients may strongly vary as a function of angle. Therefore, to achieve omnidirectional coherent absorption, for any bilateral source distribution, we further require R and T to be angle independent. In the main text, we have considered the case of TM-polarized bilateral illumination with $\Delta\phi = \pi$, which, according to the above discussion, requires a CPA structure with scattering matrix of the form of Eq. (A15). In particular, we have chosen to implement a scattering matrix as in Eq. (A15) with $c = 1/2$:

$$S_{\mathrm{CPA}} = \frac{1}{2}\begin{pmatrix} -1 & 1 \\ 1 & -1 \end{pmatrix} \quad \forall\ \theta. \tag{B6}$$

It should be noted that the specific values of R and T (i.e., the value of c) can be chosen arbitrarily, as long as Eq. (B4), or (B5), is fulfilled (even if they lead to a nonpassive structure). The only forbidden values for R and T are the ones that lead to an ideally lossless structure (i.e., any complex R and T for which $|R|^2 + |T|^2 = 1$) since CPA operation always requires a finite amount of absorption. However, as long as Eq. (B4), or (B5), is fulfilled, this amount of absorption can be made arbitrarily small. This is not surprising, as a CPA is based not only on material absorption but also on destructive interference. Interestingly, this also means that there is no fundamental lower bound on the level of loss or gain necessary for the operation of the proposed PT-symmetric lens.

Further details on the design of the specific CPA structure considered in the main text are provided in Ref. [36].

APPENDIX C: LOSSY DNG LENS VS PT-SYMMETRIC LENS

One of the main advantages of the proposed PT-symmetric lens is its loss-immune response. More specifically, material losses are a fundamental ingredient of the PT-symmetric lensing mechanism. Conversely, in typical metamaterial flat lenses, such as DNG lenses, material absorption is strongly detrimental for the performance of the device; therefore, in conventional metamaterial implementations, the goal is always to reduce losses as much as possible. Unfortunately, since metamaterials are typically based on the resonant response of their subwavelength inclusions, material absorption is unavoidable because losses are fundamentally associated with frequency dispersion through Kramers-Kronig relations [29]. In order to visually appreciate the effect of absorption, in Fig. 7 we compare the field-intensity distribution of the PT-symmetric lens presented in the main text with that of a lossy DNG lens. In particular, we chose the relative permittivity and permeability of the DNG material as $\varepsilon_{\mathrm{DNG}} = -1 + 0.02i$ and $\mu_{\mathrm{DNG}} = -1 + 0.02i$, in which the imaginary part has been chosen to be similar to that of the permittivity of silver, when its real part is -1. It should be noted that this is an "optimistic" choice for the

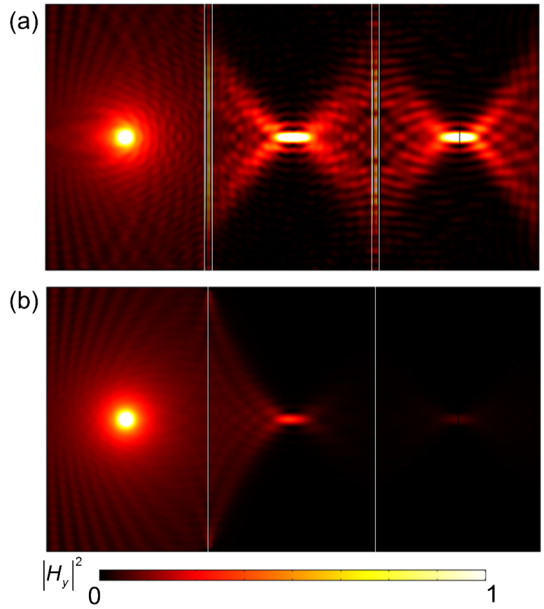

FIG. 7. Field-intensity distribution of (a) the proposed PT-symmetric lens, as in Figs. 3 and 4, and (b) a lossy DNG lens (located between the two vertical white lines).

metamaterial losses since silver has arguably the lowest level of losses among materials with small and negative permittivity at optical frequencies [43]. Nevertheless, it is clear from Fig. 7(b) that material absorption almost completely suppresses the image produced by the DNG lens, as the fields strongly decay inside the material (besides, subwavelength resolution is not achievable in this case since the evanescent spectrum also decays inside the DNG slab). Conversely, in the proposed PT-symmetric lens, thanks to the interplay of loss and gain, the intensity of the image is very high, comparable to the intensity of the source, as seen in Fig. 7(a).

[1] M. Born and E. Wolf, *Principles of Optics: Electromagnetic Theory of Propagation, Interference and Diffraction of Light* (Cambridge University Press, Cambridge, England, 1999).

[2] J. C. Maxwell, *On the General Laws of Optical Instruments*, Q. J. Pure Appl. Math. **II**, 271 (1858).

[3] A. Walther, *Irreducible Aberrations of a Lens Used for a Range of Magnifications*, J. Opt. Soc. Am. A **6**, 415 (1989).

[4] T. Smith, *On Perfect Optical Instruments*, Proc. Phys. Soc. London **60**, 293 (1948).

[5] Interestingly, while a plane mirror was the only known example of a planar absolute optical instrument before the advent of metamaterials, different nonplanar spherically symmetric absolute instruments are well known in classical optics, most notably the Maxwell's fish-eye lens, variants of the Luneberg lens, etc. [1,6].

[6] T. Tyc, L. Herzánová, M. Šarbort, and K. Bering, *Absolute Instruments and Perfect Imaging in Geometrical Optics*, New J. Phys. **13**, 115004 (2011).

[7] V. G. Veselago, *The Electrodynamics of Substances with Simultaneously Negative Values of ε and μ*, Sov. Phys. Usp. **10**, 509 (1968).

[8] J. B. Pendry, *Negative Refraction Makes a Perfect Lens*, Phys. Rev. Lett. **85**, 3966 (2000).

[9] V. A. Podolskiy and E. E. Narimanov, *Near-Sighted Superlens*, Opt. Lett. **30**, 75 (2005).

[10] X.-X. Liu and A. Alu, *Limitations and Potentials of Metamaterial Lenses*, J. Nanophoton. **5**, 053509 (2011).

[11] A. Grbic and G. Eleftheriades, *Overcoming the Diffraction Limit with a Planar Left-Handed Transmission-Line Lens*, Phys. Rev. Lett. **92**, 117403 (2004).

[12] S. Maslovski and S. Tretyakov, *Phase Conjugation and Perfect Lensing*, J. Appl. Phys. **94**, 4241 (2003).

[13] J. B. Pendry, *Time Reversal and Negative Refraction*, Science **322**, 71 (2008).

[14] M. Notomi, *Theory of Light Propagation in Strongly Modulated Photonic Crystals: Refractionlike Behavior in the Vicinity of the Photonic Band Gap*, Phys. Rev. B **62**, 10696 (2000).

[15] C. Luo, S. Johnson, J. Joannopoulos, and J. Pendry, *All-Angle Negative Refraction without Negative Effective Index*, Phys. Rev. B **65**, 201104 (2002).

[16] D. R. Smith, D. Schurig, J. J. Mock, P. Kolinko, and P. Rye, *Partial Focusing of Radiation by a Slab of Indefinite Media*, Appl. Phys. Lett. **84**, 2244 (2004).

[17] A. Poddubny, I. Iorsh, P. Belov, and Y. Kivshar, *Hyperbolic Metamaterials*, Nat. Photonics **7**, 948 (2013).

[18] R. Fleury, D. L. Sounas, and A. Alù, *Negative Refraction and Planar Focusing Based on Parity-Time Symmetric Metasurfaces*, Phys. Rev. Lett. **113**, 023903 (2014).

[19] C. M. Bender and S. Boettcher, *Real Spectra in Non-Hermitian Hamiltonians Having PT Symmetry*, Phys. Rev. Lett. **80**, 5243 (1998).

[20] K. G. Makris, R. El-Ganainy, D. N. Christodoulides, and Z. H. Musslimani, *Beam Dynamics in PT Symmetric Optical Lattices*, Phys. Rev. Lett. **100**, 103904 (2008).

[21] C. E. Rüter, K. G. Makris, R. El-Ganainy, D. N. Christodoulides, M. Segev, and D. Kip, *Observation of Parity–Time Symmetry in Optics*, Nat. Phys. **6**, 192 (2010).

[22] S. Longhi, *PT-Symmetric Laser Absorber*, Phys. Rev. A **82**, 031801 (2010).

[23] Z. Lin, H. Ramezani, T. Eichelkraut, T. Kottos, H. Cao, and D. N. Christodoulides, *Unidirectional Invisibility Induced by PT-Symmetric Periodic Structures*, Phys. Rev. Lett. **106**, 213901 (2011).

[24] H. Hodaei, M.-A. Miri, M. Heinrich, D. N. Christodoulides, and M. Khajavikhan, *Parity-Time-Symmetric Microring Lasers*, Science **346**, 975 (2014).

[25] X. Zhu, H. Ramezani, C. Shi, J. Zhu, and X. Zhang, *PT-Symmetric Acoustics*, Phys. Rev. X **4**, 031042 (2014).

[26] R. Fleury, D. L. Sounas, and A. Alù, *An Invisible Acoustic Sensor Based on Parity-Time Symmetry*, Nat. Commun. **6**, 5905 (2015).

[27] D. L. Sounas, R. Fleury, and A. Alù, *Unidirectional Cloaking Based on Metasurfaces with Balanced Loss and Gain*, Phys. Rev. Applied **4**, 014005 (2015).

[28] In classical electrodynamics, a nonlocal response is equivalent to spatial dispersion (see, for example, Ref. [29]). In general, if the value of permittivity $\varepsilon(\mathbf{k})$, is a function of the wave number $\mathbf{k}$, then in the Fourier space the displacement field $\mathbf{D}$ is related to the electric field $\mathbf{E}$ through $\mathbf{D}(\mathbf{k}) = \varepsilon(\mathbf{k})\mathbf{E}(\mathbf{k})$. Taking the Fourier transform of this relation one finds $\tilde{\mathbf{D}}(\mathbf{r}) = \int \tilde{\varepsilon}(\mathbf{r}-\mathbf{r}')\tilde{\mathbf{E}}(\mathbf{r}')d\mathbf{r}'$, where the tilde indicates quantities in real space, and $\mathbf{r}$ is the position vector. It is obvious, therefore, that a permittivity function of the wave number (spatially dispersive) implies a response that is a function of a finite region of space, not only a point (nonlocal response).

[29] L. D. Landau, L. P. Pitaevskii, and E. M. Lifshitz, *Electrodynamics of Continuous Media*, 2nd ed. (Butterworth-Heinemann, Oxford, 1984).

[30] Y. D. Chong, L. Ge, H. Cao, and A. D. Stone, *Coherent Perfect Absorbers: Time-Reversed Lasers*, Phys. Rev. Lett. **105**, 053901 (2010).

[31] W. Wan, Y. Chong, L. Ge, H. Noh, A. D. Stone, and H. Cao, *Time-Reversed Lasing and Interferometric Control of Absorption*, Science **331**, 889 (2011).

[32] C. M. Watts, X. Liu, and W. J. Padilla, *Metamaterial Electromagnetic Wave Absorbers*, Adv. Mater. **24**, OP98 (2012).

[33] C. Argyropoulos, *Electromagnetic Absorbers Based on Metamaterial and Plasmonic Devices*, FERMAT **2** (2014).

[34] C. A. Valagiannopoulos, A. Tukiainen, T. Aho, T. Niemi, M. Guina, S. A. Tretyakov, and C. R. Simovski, *Perfect Magnetic Mirror and Simple Perfect Absorber in the Visible Spectrum*, Phys. Rev. B **91**, 115305 (2015).

[35] A. Silva, F. Monticone, G. Castaldi, V. Galdi, A. Alù, and N. Engheta, *Performing Mathematical Operations with Metamaterials*, Science **343**, 160 (2014).

[36] See Supplemental Material at http://link.aps.org/supplemental/10.1103/PhysRevX.6.041018 for further details on the design of the omnidirectional CPA structure, a discussion of the robustness of the proposed design to small perturbations, a simplified design with relaxed parameters, as well as an analysis of the transient response of a dispersive PT-symmetric lens and its stability. Supplemental Material also includes time-harmonic animations of the field distributions in Figs. 2 and 3, and animations of the field distributions in the transient regime, for an example of a dispersive PT-symmetric lens, under plane-wave and point-source illuminations.

[37] All the field distributions at steady state presented in this paper and in Ref. [36] have been numerically calculated with the commercial finite-element software COMSOL Multiphysics. The field distributions in the transient regime have been calculated with an in-house 2D time-dispersive FDTD engine.

[38] It should be noted that only a phase difference $\Delta\phi = 0, \pi, 2\pi, \ldots$ guarantees ideal imaging in the sense of Eq. (1), consistent with the fact that a symmetric structure can realize CPA operation only for symmetric or antisymmetric illumination, as shown in Appendix B and Ref. [30]. The generalization of these results to nonsymmetric CPAs and arbitrary phase delay $\Delta\phi$, which may realize other interesting wave-manipulation functionalities (different from ideal imaging), is discussed in [39].

[39] C. A. Valagiannopoulos, F. Monticone, and A. Alù, *PT-Symmetric Planar Devices for Field Transformation and Imaging*, J. Opt. **18**, 044028 (2016).

[40] F. Monticone, N. M. Estakhri, and A. Alù, *Full Control of Nanoscale Optical Transmission with a Composite Metascreen*, Phys. Rev. Lett. **110**, 203903 (2013).

[41] N. Yu and F. Capasso, *Flat Optics with Designer Metasurfaces*, Nat. Mater. **13**, 139 (2014).

[42] D. M. Pozar, *Microwave Engineering*, 3rd ed. (Wiley, New York, 2011).

[43] P. B. Johnson and R. W. Christy, *Optical Constants of the Noble Metals*, Phys. Rev. B **6**, 4370 (1972).